Furnace vestibule heat transport models

M. J. McGuinness[1] B. J. Cox[2] B. Kalyanaraman[3]
K. B. Kiradjiev[4] R. Gonzalez-Farina[5]
C. Z. W. Hassell Sweatman[6] Lindon Roberts[7]
D. I. Pontin[8] Edward J. Bissaker[9] S. K. Irvine[10]
D. R. Jenkins[11] I. J. Taggart[12]

(Received 11 July 2021; revised 18 February 2023)

Abstract

This is a report on the Lovells Springs challenge that was brought to the Mathematics in Industry Study Group at the University of Newcastle, Australia, in January 2020. The design of a furnace that heats steel rods to make them malleable and allow the reshaping of the rods into coiled springs is the challenge. Mathematical modelling of heat transport in the half-metre long furnace vestibule predicts the effect of vestibule geometry on the temperature of rods entering the furnace, and provides guidelines for deciding on the dimensions of the vestibule for improved energy efficiency of heating. Models considered include treating the rods as equivalent steel sheets, and as discrete steel rods. The relative importance of radiative and convective heat transfer

DOI:10.21914/anziamj.v62.16642, © Austral. Mathematical Soc. 2023. Published 2023-02-28, as part of the Proceedings of the 2020 Mathematics and Statistics in Industry Study Group. ISSN 1445-8810. (Print two pages per sheet of paper.) Copies of this article must not be made otherwise available on the internet; instead link directly to the DOI for this article.

mechanisms is considered. A longer vestibule, with length one or two metres, is recommended for improved heating efficiency of rods thicker than 25mm.

Contents

1 Introduction **M113**

2 Advective heat transport **M115**
2.1 Analytic solutions M118
2.2 Numerical simulations M119

3 View aspect calculation **M124**
3.1 View factor for simplified geometries M124
3.2 View factor for more realistic geometries M126

4 Simulations for steel rods **M129**

5 Heat transfer in the base **M135**
5.1 Model formulation M139
5.2 Numerical solution M141
5.3 Results M142
5.4 Conclusions M151

6 Conclusions **M152**

1 Introduction

This is a report on the challenge brought to the 2020 Mathematics in Industry Study Group by Simon Crane, Lovells Springs, at the University of Newcastle in Australia.

Lovells is a world leader and a world specialist in the manufacture of suspension coils. During the manufacturing process steel rods of a circular cross section must be heated to temperatures in excess of 800 °C so they become malleable for machines to twist into coils. Currently the heating of these rods takes place in a large furnace. The heat source is a fireball of burning natural gas and compressed air injected into the furnace. Temperatures in the main chamber exceed 1000 °C. Lovells is planning the construction of a new furnace and require a mathematical model that demonstrates the key factors to reduce heat loss and improve the overall furnace efficiency. In particular, Lovells seek insight into possible ways of better utilising hot waste gases to heat rods in the vestibule (the entry section of the furnace) prior to firing in the main chamber.

The spacing between rods, and the length of the vestibule leading to the furnace, are key parameters. While the original problem statement includes a model of the whole system of furnace and vestibule, the industry representative later asked the group to focus on the thermal processes in the vestibule.

The following describes the set-up for the furnaces presently used by Lovells, which are used for the modelling as a basis for suggesting changes that should improve energy efficiency. With reference to the sketch of a typical furnace in Figure 1, ambient temperature steel bars enter the furnace from the right via a 0.5 m long vestibule. The existing furnaces are 2–8 m long (in a direction perpendicular to the page in the sketch), and are essentially a box with insulating walls and a floor that is scalloped to hold the rods. Rods are advanced through the furnace by a conveyor mechanism that periodically shifts (walks) them, all together, through the vestibule and the furnace. The total time that each rod spends in the furnace is set by the operator, and varies from seven minutes to one hour, with the longer times chosen for thicker rods with diameters up to 57 mm, and the shorter times for thinner rods down to 16 mm diameter.

In the remainder of this report, we build a collection of models of increasing sophistication describing the heating of the rods, with a particular focus on

Figure 1: Schematic of furnace in section view with flames heating the larger compartment to 1100°C, steel rods entering via the vestibule from the right, and exiting after heating on the left.

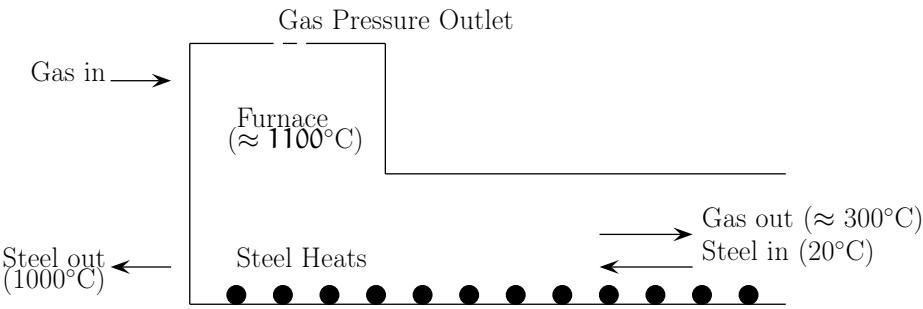

what happens in the entry vestibule of a furnace. In Section 2 a simplified geometry is adopted with rods approximated as sheets of steel, and with heating driven by gas advection only. We then derive analytic solutions in the case of constant material properties. Cases where material properties are allowed to vary with temperature are solved numerically. Section 3 derives and analyses expressions for radiative heat transfer based on the geometry of the furnace system. The heating model is then extended in Section 4 to include discrete rods of finite width. Quasi-steady numerical solutions account for both radiative heat transfer and the stop-start motion of the rods. Lastly, Section 5 extends to a model that also includes the heating effects and gas loss at the base of the furnace.

2 Advective heat transport

In this model we adopt a simplified geometry where we have a vestibule of height H and length L. The vertical direction is divided into a gas region of

height ℓ_g, and a steel sheet of thickness ℓ_s that moves through the furnace at the same speed as the rods, so that $H = \ell_g + \ell_s$. We assume here that the velocity of gas advection v_g is of sufficient magnitude that advection dominates the transport of thermal energy, and other mechanisms (such as radiation) are ignored in this simple first approach to modelling the vestibule. The steel is conceptualised in this preliminary model as an equivalent steel slab. Since the steel is not in reality a slab but a series of rods, we neglect the effects of thermal energy transport in the steel due to diffusion within the steel. The steel advances towards the furnace at an externally imposed velocity of v_s. The transport of thermal energy from the hotter gas to the cooler steel is modelled with a Newton heating/cooling term where the coefficient of heat transfer is denoted by h. The principal material properties of the gas and the steel needed to account for the transport of thermal energy are the densities ρ and specific heats c, to which we apply the subscript g or s to denote gas or steel.

Heat, gas, and steel motion are considered to take place in one space and one time dimension, so that $T_g(x,t)$ and $T_s(x,t)$. The origin is positioned at the junction between furnace and vestibule, with x increasing towards the cold end of the vestibule. Advection is assumed to be more important than diffusion for heat transport in the x-direction, and the heat exchange between gas and steel is taken to be such that

$$\frac{\partial T_g}{\partial t} = -v_g \frac{\partial T_g}{\partial x} - \frac{h}{\rho_g c_g \ell_g}(T_g - T_s), \tag{1a}$$

$$\frac{\partial T_s}{\partial t} = -v_s \frac{\partial T_s}{\partial x} + \frac{h}{\rho_s c_s \ell_s}(T_g - T_s), \tag{1b}$$

together with the boundary values $T_g|_{x=0} = T_{fce}$ and $T_s|_{x=L} = T_{amb}$, where T_{fce} and T_{amb} are the temperatures inside and outside of the furnace, respectively. Tables 1 and 2 list nomenclature, units, and typical values for physical constants.

Now considering the steady-state, $T_g(x,t) = T_g(x)$ and $T_s(x,t) = T_s(x)$, equations (1a) and (1b) become the system of ordinary differential equations

Table 1: Nomenclature where the subscript $j \in \{g, s, b\}$ denotes gas, steel and base (floor of vestibule) material, respectively

Symbol	Name	Units
c_j	Specific heat of j	$\mathrm{J\,kg^{-1}\,K^{-1}}$
h	Heat transfer coefficient	$\mathrm{J\,s^{-1}\,m^{-2}.K^{-1}}$
k	Thermal conductivity	$\mathrm{W\,m^{-1}\,K^{-1}}$
t	Time dimension	s
T_j	Temperature of j	K
v_j	Velocity of j	$\mathrm{m\,s^{-1}}$
x, y, z	Spatial dimensions	m
ϵ	Emissivity	dimensionless
κ	Thermal diffusivity	$\mathrm{m^2/s}$
μ	Dynamic viscosity	Pa s
ρ_j	Density of j	$\mathrm{kg\,m^{-3}}$

Table 2: Table of constants used in models

Symbol	Name	Value	Units
c_g	Specific heat of gas	0.6	$\mathrm{kg\,m^{-3}}$
c_s	Specific heat of steel	8000	$\mathrm{kg\,m^{-3}}$
H	vestibule height	0.1	m
ℓ_j	length scale for material j	$\ell_s = 0.01$	m
L	vestibule length	0.5	m
Nu	Nusselt number	64	dimensionless
P_g	Pressure of gas	10^5	Pa
R	Ideal gas constant	8.314	$\mathrm{J\,mol^{-1}\,K^{-1}}$
ρ_g	Density of gas (water vapour)	0.6	$\mathrm{kg\,m^{-3}}$
ρ_s	Density of steel	7854	$\mathrm{kg\,m^{-3}}$
σ	Stefan–Boltzmann constant	$5.670 \cdot 10^{-8}$	$\mathrm{W\,m^{-2}\,K^{-4}}$

(ODEs)

$$v_g \rho_g c_g \ell_g T_g' + h(T_g - T_s) = 0\,, \tag{2a}$$
$$v_s \rho_s c_s \ell_s T_s' - h(T_g - T_s) = 0\,, \tag{2b}$$

where primes denote differentiation with respect to x. We denote $\alpha_g = v_g \rho_g c_g \ell_g$, and $\alpha_s = v_s \rho_s c_s \ell_s$, to give the ODEs

$$\alpha_g T_g' + h(T_g - T_s) = 0\,, \tag{3a}$$
$$\alpha_s T_s' - h(T_g - T_s) = 0\,. \tag{3b}$$

2.1 Analytic solutions

Adding equations (3a) and (3b) gives $\alpha_g T_g' + \alpha_s T_s' = 0$, which (provided the α_j coefficients are constant) is immediately integrated to yield $\alpha_g T_g + \alpha_s T_s = (\alpha_g + \alpha_s) C_1$, for some constant of integration C_1. Solving this for the temperature in the steel gives $T_s = \frac{1}{\alpha_s}\left[(\alpha_g + \alpha_s) C_1 - \alpha_g T_g\right]$. Substituting this into equation (3a) leads to $\alpha_g T_g' + \beta \left\{ T_g - \frac{1}{\alpha_s}\left[(\alpha_g + \alpha_s) C_1 - \alpha_g T_g\right] \right\} = 0$, which is now a single ODE for $T_g(x)$. Simplifying this ODE we write it as $T_g' + \gamma(T_g - C_1) = 0$, where $\gamma = h(\alpha_g + \alpha_s)/(\alpha_g \alpha_s)$. This final ODE is a first-order variables separable equation with the general solution

$$T_g = C_1 + C_2 e^{-\gamma x}, \quad \text{and then} \quad T_s = C_1 - C_2 \frac{\alpha_g}{\alpha_s} e^{-\gamma x}$$

is therefore the corresponding solution for the temperature in the steel. Now consider the boundary conditions: $T_g|_{x=0} = T_{fce}$ determines $T_{fce} = C_1 + C_2$; and $T_s|_{x=L} = T_{amb}$ yields $T_{amb} = C_1 - C_2 \frac{\alpha_g}{\alpha_s} e^{-\gamma L}$. This linear system of two equations in two unknowns determines

$$C_1 = T_{fce} - \frac{T_{fce} - T_{amb}}{1 + \frac{\alpha_g}{\alpha_s} e^{-\gamma L}}\,, \quad C_2 = \frac{T_{fce} - T_{amb}}{1 + \frac{\alpha_g}{\alpha_s} e^{-\gamma L}}\,.$$

This provides an approximate analytic solution to the problem being modelled under the further assumption that all the material properties remain constant for the range of temperature under consideration. Figure 2 graphs these solutions when $v_g = 0.25\,\mathrm{m/s}$. Also see Figures 3 and 4 for further illustrations of the implications of the analytic solution for temperatures of the gas and steel where they exit the vestibule, and how those temperatures are affected by velocities and vestibule geometry.

The next subsection has further extensions to the model where the assumption of constant material properties is not made. In particular we replace the heat transfer coefficient h with a quadratic function of the gas temperature T_g and we replace the specific heat of the steel c_s with a linear function of the steel temperature T_s. We then compute numerical solutions to equations (3a) and (3b) with non-constant properties and heat transfer coefficient. With these extensions, solutions are explored using numerical schemes. The analytical solution presented above provides an initial 'guess' which is very useful for numerical schemes that solve boundary value problems like this one.

2.2 Numerical simulations

We now extend the previous subsection by accounting for variable properties of steel and gas. First we note a conservation result that applies for both constant and non-constant material properties.

Conservation of mass in the steady state for the gas implies that if the vestibule has constant cross-section area A, then the product $\rho_g(T_g)v_g(T_g)$ is a constant. This follows because the steady-state assumption implies that mass flux of exhaust gas per unit time along the vestibule is constant. Gas mass is $m = \rho_g V$, where V denotes gas volume. Then conservation of mass says that for an arbitrary region in the vestibule and over some arbitrary time interval, the mass of gas flowing in must match the mass of gas flowing out, since otherwise the amount of gas in that region would be changing with

Figure 2: Solutions to the steady-state sheet steel vestibule model with no radiative transport. Temperatures (versus distance from the furnace along the vestibule) from analytic solutions for constant coefficients in Section 2.1 are compared with temperatures from numerical solutions to the boundary-value problem for non-constant coefficients in Section 2.2. Gas velocity is $0.25\,\mathrm{m/s}$.

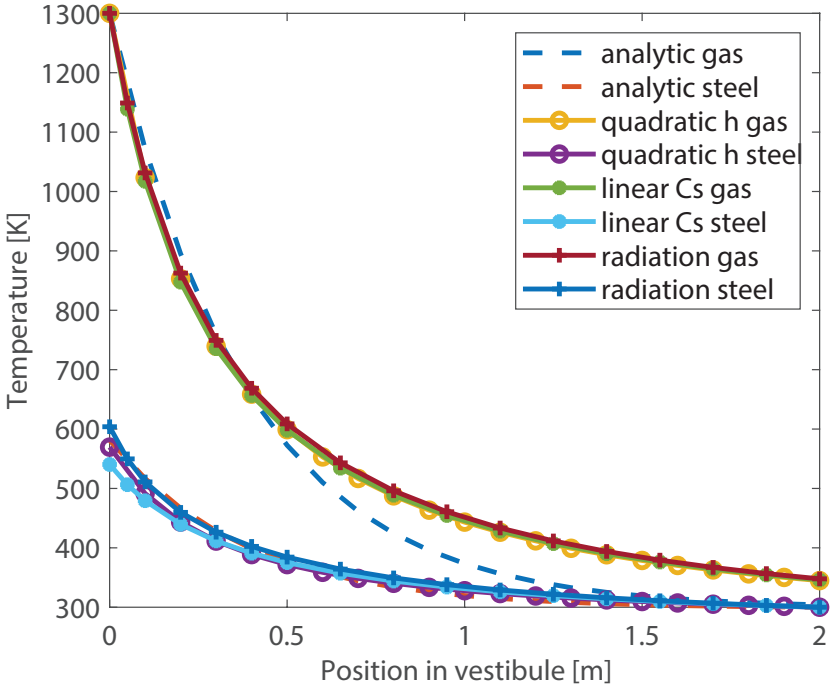

Figure 3: Numerical results for the steady-state model with no radiation, showing the gas temperature at $x = L$ where it exits the vestibule (solid blue line), and steel temperature at $x = 0$ where it enters the furnace from the vestibule (dashed red line), versus vestibule height H, steel thickness or height ℓ_s, gas velocity at $x = 0$, and steel velocity.

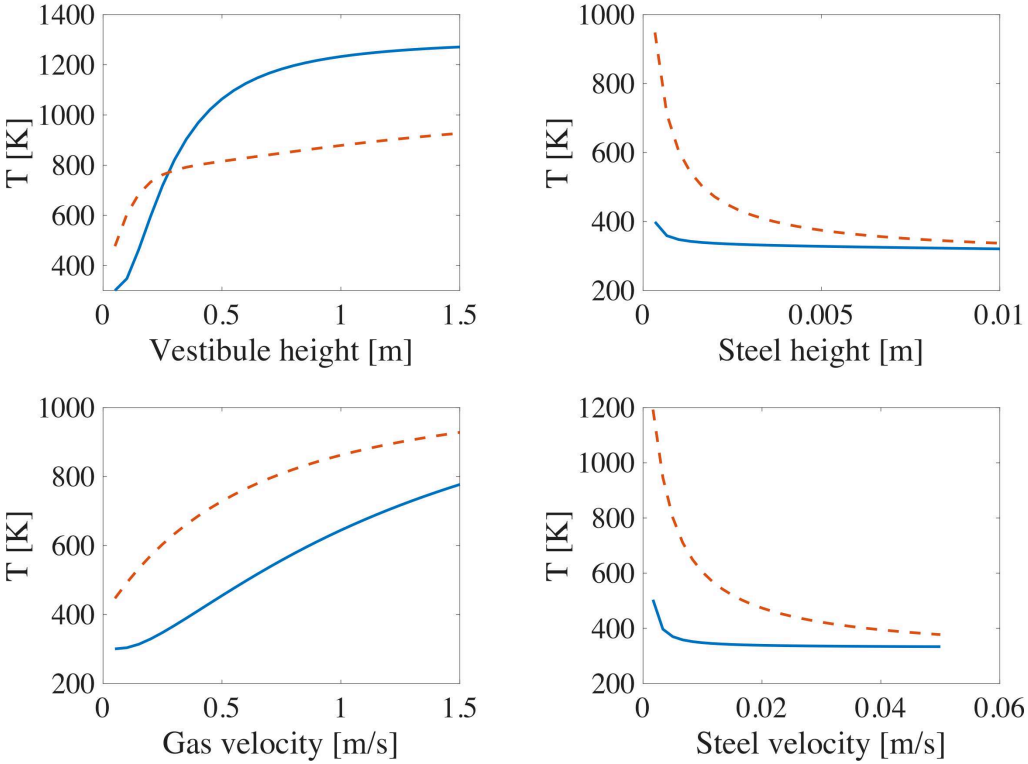

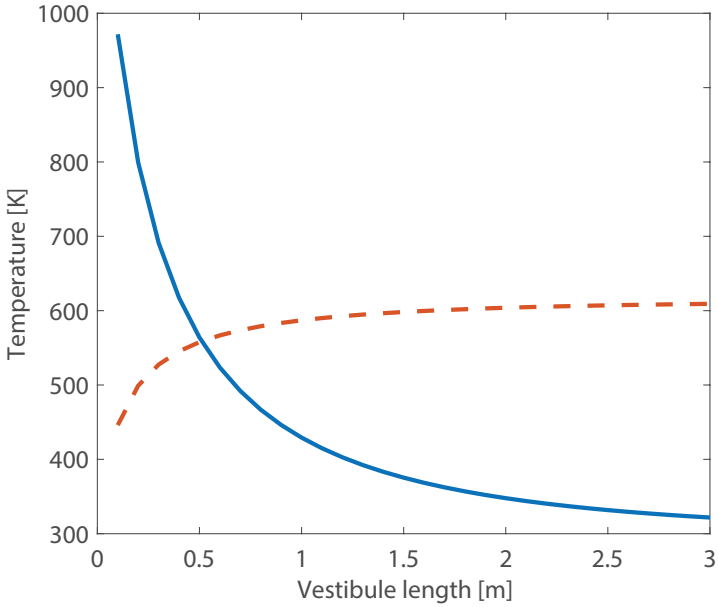

Figure 4: Numerical results for the steady-state model with no radiation, showing the gas temperature at $x = L$ where it exits the vestibule (solid blue line), and steel temperature at $x = 0$ where it enters the furnace from the vestibule (dashed red line), versus vestibule length L.

time. It follows that

$$\rho_{in} v_{in} A = \rho_{out} v_{out} A\,, \quad \text{or} \quad \rho_{in} v_{in} = \rho_{out} v_{out}\,,$$

where v is gas velocity and ρ is gas density.

So the product $\rho_g v_g$ is constant for exhaust gases, along the vestibule, despite the dramatic changes in gas temperature expected. The industry representative indicated that pressures in the exhaust region are close to atmospheric pressure.

A similar result holds for the steel, although steel density changes are negligible with temperature for heat transport purposes, unlike the exhaust gases. So the result reduces to a constant steel velocity, which is a condition imposed by the furnace setup.

The thermal conductivity of carbon dioxide is (Gupta and Saxena 1970)

$$k_g(T_g) = 418.4 \cdot 10^{-5}\big(-2.400 + 2.16 \cdot 10^{-2} T_g - 3.244 \cdot 10^{-6} T_g^2\big).$$

The thermal conductivity of steel is $k_s = mT_s + c$ in $\mathrm{W\,m^{-1}\,K^{-1}}$ (Gupta and Saxena 1970). This linear relationship is calibrated by two measurements (Sweatman, Barry, and McGuinness 2012). We use $m = -30/700 \approx -0.043$ and $c = 60 + 30 \times (300/700) \approx 73$. Gas pressure is to a good approximation always at atmospheric pressure, $P_g = 10^5\,\mathrm{Pa}$. The density of gas is taken from that for carbon dioxide using the ideal gas law $PV = nRT$, giving $\rho_g = 44 \times 10^{-3} \times P_g/(RT_g)$. The convective heat transfer coefficient is h, and the Nusselt number definition provides $h = \mathrm{Nu}\,k_g/\ell_g$ so h depends on T_g through k_g . The specific heat capacity of gas is here taken to be $c_g = 1100\,\mathrm{J\,kg^{-1}\,K^{-1}}$. The specific heat capacity of steel can be approximated as $c_s = 500\,\mathrm{J\,kg^{-1}\,K^{-1}}$, whereas a more accurate value depends on the temperature of the steel, $c_s = 1.05T_s + 119$. This was obtained by fitting to values presented by Sweatman, Barry, and McGuinness (2012). For a gas velocity of $1\,\mathrm{m\,s^{-1}}$ at $x = 0$, we take the constant value for ρv to be 0.4071. For steel, we take $\rho_s(T_s)v_s(T_s) = 78.54$

The steady-state equations (2a) and (2b) are solved numerically for variable coefficients with boundary conditions $T_g = 1300\,\mathrm{K}$ at $x = 0$, and $T_s = 300\,\mathrm{K}$ at $x = L$. This can be done by using an initial-value differential equation solver in MATLAB like `ode45`, setting $T_g = 1300\,\mathrm{K}$ at $x = 0$, and shooting by hand on the temperature in the steel at $x = 0$ until the desired value is obtained at $x = L$. An alternative that is easier to code and that gives the same results is to use a boundary value problem solver like `bvp4c` in MATLAB. This solver does the shooting automatically and successfully, provided a suitable guess for the initial temperature profile is chosen.

We present results using the less accurate case that the coefficient of thermal capacity for steel is assumed to be fixed at $c_s = 500$ in Figure 2, for a gas velocity of $0.25\,\mathrm{m/s}$. Figure 2 also plots results that use the more accurate linear dependence of c_s on temperature. We summarise the implications of the results and figures in this section as follows.

- Whatever the gas velocity, a longer vestibule allows for more heat transfer. Slower velocities require shorter vestibules to attain the same

exit gas temperature. Hence, for faster gas velocity allow for a longer vestibule.

- If trying to pre-heat the bars to a higher temperature in the vestibule, then a faster-flowing gas in a long vestibule gives a better result. However, faster gas exits at higher temperatures than a slower gas.
- If trying to cool the gas by heat exchange, then a slow gas with a long vestibule gives a better result. However, bars then enter the furnace at cooler temperatures than for a faster gas.
- The more accurate model using $c_s(T_s)$ predicts lower steel temperatures at the hot end of the vestibule, than does the model using the approximate fixed value $c_s = 500\,\mathrm{J\,kg^{-1}\,K^{-1}}$.
- Radiation from furnace to vestibule is not yet taken into account.

3 View aspect calculation

3.1 View factor for simplified geometries

This section derives an expression for the view factor for radiative heat transfer to and from the steel in the thin slab model from Section 2.1. With reference to Figure 5, we compute the view factor from Nusselt analogue, where we centre an idealised sphere at a typical area element on the steel surface ds, with a radius $r = 1/(2\sqrt{\pi})$, so that the total spherical area is one. By assuming that the area element is located so that the furnace extends into and out of the page to an extent that edge effects can be ignored, then the integrals we need to compute are

$$\theta_{\mathrm{fce}} = \frac{1}{4\pi}\int_0^{\phi_{\mathrm{fce}}}\int_{-\pi}^{\pi} \sin\theta\,d\theta\,d\phi\,, \quad \theta_{\mathrm{amb}} = \frac{1}{4\pi}\int_0^{\phi_{\mathrm{amb}}}\int_{-\pi}^{\pi} \sin\theta\,d\theta\,d\phi\,,$$

Figure 5: View factor for the simplified geometry based on the Nusselt analogue. The area of the spherical shells are calculated from a idealised sphere centred at ds with unit total area (i.e., radius $r = 1/(2\sqrt{\pi})$).

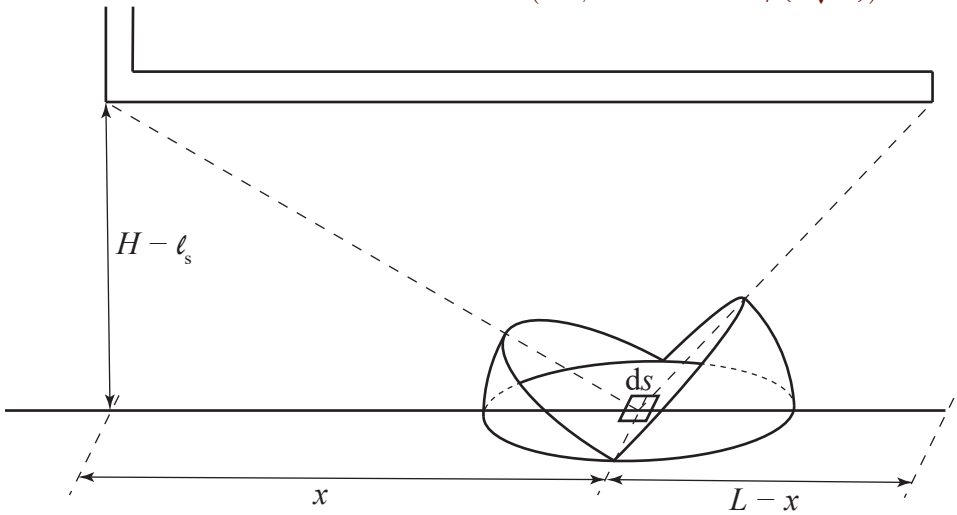

where $\phi_{fce} = \tan^{-1} \frac{H-\ell_s}{x}$, and $\phi_{amb} = \tan^{-1} \frac{H-\ell_s}{L-x}$. These integral expressions are readily evaluated to give

$$\theta_{fce} = \frac{1}{4}\left[1 - \frac{x}{\sqrt{(H-\ell_s)^2 + x^2}}\right],$$

$$\theta_{amb} = \frac{1}{4}\left[1 - \frac{L-x}{\sqrt{(H-\ell_s)^2 + (L-x)^2}}\right].$$

In this geometrically simplified model we assume that the radiative term affects the steel only which is made up of two components. Firstly there is the positive heating term which accounts for the increase of thermal energy resulting from interactions with the furnace, and secondly there is a loss of thermal energy through interactions with the ambient environment outside of the vestibule. The interactions with the vestibule roof and the ground is

assumed to be in equilibrium and lead to no net change to the thermal energy in the steel. Under these assumptions then we update the governing PDE for the temperature in the steel to read

$$\frac{\partial T_s}{\partial t} = -v_s \frac{\partial T_s}{\partial x} + \frac{h}{\rho_s c_s \ell_s}(T_g - T_s) + \frac{\epsilon\sigma}{\rho_s c_s \ell_s}\left[\theta_{fce} T_{fce}^4 + \theta_{amb} T_{amb}^4 - (\theta_{fce} + \theta_{amb}) T_s^4\right],$$

where ϵ is the emissivity of the steel and σ is the Stefan–Boltzmann constant. For standard operation of the furnaces at Lovells, the term involving T_{amb} can take values that are of the same order as the term involving T_{fce} near the vestibule entrance, and so we include both terms in the numerical results that follow.

3.2 View factor for more realistic geometries

In this section, we model radiative heat transfer between the rods in the vestibule. To simplify the problem, we assume that the geometries involved are two-dimensional and the rods are modelled as vertical slabs instead of cylinders. The schematic is shown in Figure 6. Let n denote the index of the position of the rod, with $n = 0$ corresponding to the rod at the boundary between the furnace and the vestibule. Let w denote the width of the furnace, and H denote the height of the vestibule. The rate at which radiative heat energy is transferred from surface S_1 to surface S_2 is (Bird, Stewart, and Lightfoot 2002, §16.4)

$$Q_{1\to 2} = \sigma A_1 F_{1\to 2}(T_1^4 - T_2^4), \tag{4}$$

where A_1 is the area of surface 1, and $F_{1\to 2}$ is the view factor (Bird, Stewart, and Lightfoot 2002, §16.4), defined to be the fraction of radiation leaving surface 1 that is directly intercepted by surface 2. It takes the value

$$F_{1\to 2} = \frac{1}{A_1}\int_{S_1}\int_{S_2} \frac{\cos\theta_1 \cos\theta_2}{\pi D^2}\, dS_1\, dS_2\,.$$

Figure 6: Schematic showing the dimensions of the rods and the furnace for radiative heating. As a simplifying assumption, the rods are modelled as slabs of length d, separated by a distance s.

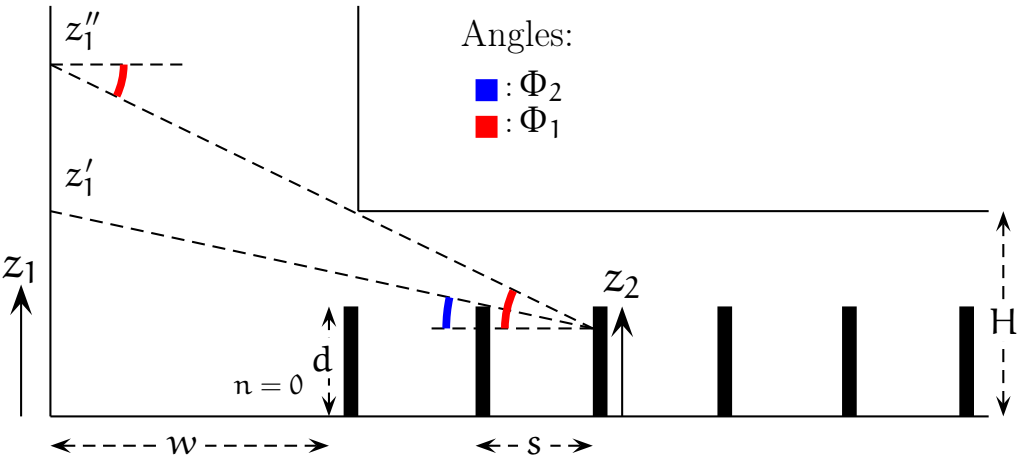

Here S_1 denote the wall of the furnace, parametrized by the variable z_1, and S_2 denotes the rod, parametrized by the variable z_2. For an arbitrary point in the rod, the angle θ_1 represents the view angle made by the rod with the wall. Since the rod and the wall are vertical, the view angle made by the wall with the rod, $\theta_2 = \theta_1$. Then the cosine

$$\cos\theta_1 = \frac{w + ns}{\sqrt{(w+ns)^2 + (z_1 - d)^2}} \approx \frac{w + ns}{\sqrt{(w+ns)^2 + z_1^2}}\,, \tag{5}$$

where z_1 is a point on the wall of the furnace. We assume that $d \ll w + ns$ and hence the separation between the points on the furnace wall and the rod is

$$D \approx \sqrt{(w+ns)^2 + z_1^2}\,. \tag{6}$$

Now to obtain the heat transfer rate (4), we need to specify the limits of integration to calculate the integral. For a given point on the rod S_2 at height z_2, we need to calculate the lowest and the highest points on the wall S_1 that are visible on the furnace, denoted by z_1' and z_1'', respectively.

From the geometry shown in Figure 6, the tangent $\tan\Phi_1 = \frac{d-z_2}{s} = \frac{z_1'-z_2}{w+ns}$. Rearranging the terms we obtain

$$z_1' = \frac{w+ns}{s}(d-z_2)+z_2\,. \tag{7}$$

Similarly, we observe that $\tan\Phi_2 = \frac{H-z_2}{ns} = \frac{z_1''-z_2}{w+ns}$, and thus

$$z_1'' = \frac{w+ns}{ns}(H-z_2)+z_2\,. \tag{8}$$

Since the area enclosed between the points z_1' and z_1'' is non-negative, we have the condition $z_1'' > z_1'$. Substituting the expressions derived in equations (7) and (8) into this inequality condition, we obtain

$$z_2 > \frac{H-nd}{1-n} = z_{2,\min}\,, \quad n>1\,, \tag{9}$$

which yields the domain of integration on the rod. Substituting the expressions (5) and (6) and the limits of integration (7) to (9) onto the heat transfer equation (4), we obtain

$$Q = \sigma(T_1^4 - T_2^4)\int_{\max(z_{2,\min},0)}^{d}\int_{z_1'}^{z_1''}\frac{(w+ns)^2}{[(w+ns)^2+z_1^2]^2}\,dz_1\,dz_2\,. \tag{10}$$

Figure 7 shows the rate of heat transfer and the temperature increase for different dimensional parameters. Observe that the rate of radiative heat transfer and the rate of temperature increase decreases with increasing distance from the furnace. Second, observe that for $s = 0.1$ m case, the heating rate decreases faster than the $s = 0.02$ m case and reaches a lower temperature

than the former within the eighth rod, due to the increase in the separation between the rods. Similar trends are observed in the temperature rate in Figure 7(b). The thermal energy input (heating rate) shown in Figure 7(c) shows heating rate as a function of the rod position for three different vestibule heights. It is observed that the radiative heat transfer is proportional to the vestibule height since more area of the vestibule is in contact with the furnace. Moreover, the heating rate is significantly higher for the $H = 0.3\,\mathrm{m}$ case than the $H = 0.12\,\mathrm{m}$ case near the furnace. This is due to more area being available for radiative heat transfer for larger vestibule heights. However, the rate quickly drops to a level comparable to the smaller values of H at larger distances from the furnace and radiation becomes a significantly less important mode of heat transfer.

4 Simulations for steel rods

This section discusses a more realistic model where the rods are modelled as separate items, with finite width as illustrated in Figure 8. The top segments carry gas, and every Kth bottom segment carries a rod (while the remaining bottom segments do not affect the model). We assume that heat transfer only occurs vertically, and that the segments are each the width of the rods (i.e., we have $N + 1$ segments in total, where $N := L/l_s$).

Within a time window, we take the positions of the rods to be fixed, and so the only processes are heat transfer into the rods and gas advection. Labelling our segments as $i = 0$ at the furnace end of the vestibule and $i = N$ at the open end, we arrive at the following (dimensional) system of ODEs. For the temperature of the gas in each segment, $T_{0,g}(t), \ldots, T_{g,N}(t)$,

$$T_{0,g}(t) = T_r, \tag{11a}$$

$$\rho_g c_g \left(\frac{dT_{i,g}}{dt} + u \frac{T_{i,g} - T_{i-1,g}}{l_s} \right) = \frac{h}{l_g}(T_{i,s} - T_{i,g}), \quad i = 1, \ldots, N, \tag{11b}$$

Figure 7: (a) Heating rate (J/s) and (b) the rate of temperature increase (K/s) as a function of rod position parameter n. The red curves are for the parameters $H = 0.3$, $w = 3$, $d = 0.01$, $s = 0.02$ and the blue curves are for the parameters $H = 0.3$, $w = 3$, $d = 0.056$, $s = 0.1$. (c) Heating rate (J/s) as a function of rod position parameter n for for vestibule heights 0.12 (squares), 0.2 (circles), and 0.3 m (asterisks). The geometric parameters are $w = 3$, $d = 0.01$, $s = 0.02$. The temperature of the furnace is $T_1 = 1000$ K and the bar temperature is $T_2 = 300$ K in all cases.

(a) Heating rate

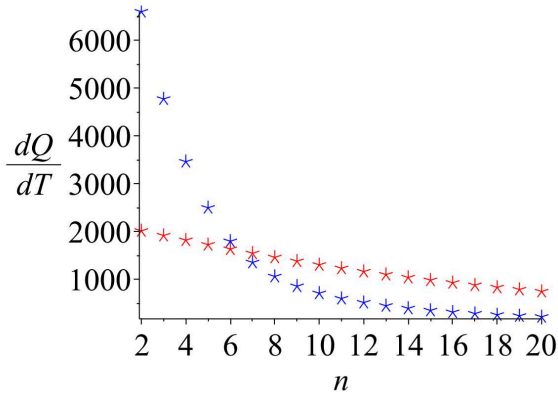

(b) Temperature rate

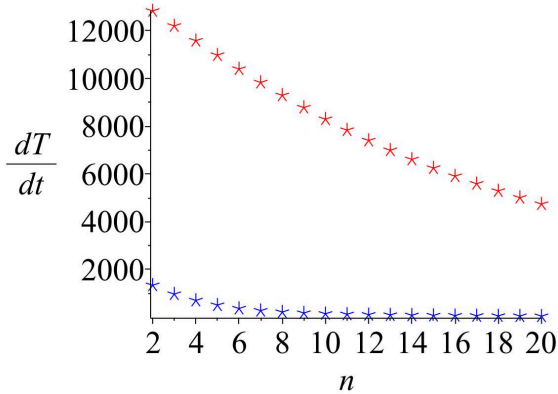

(c) Heating rate

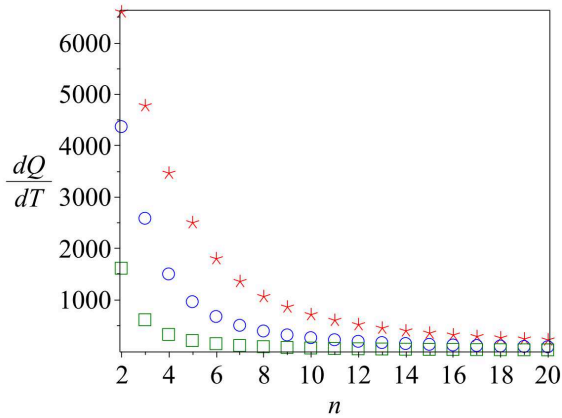

Figure 8: Diagram of discrete model with finite-width rods. The top segments carry gas T_i^g and the bottom segments carry solid T_i^s, where here every third segment has a rod.

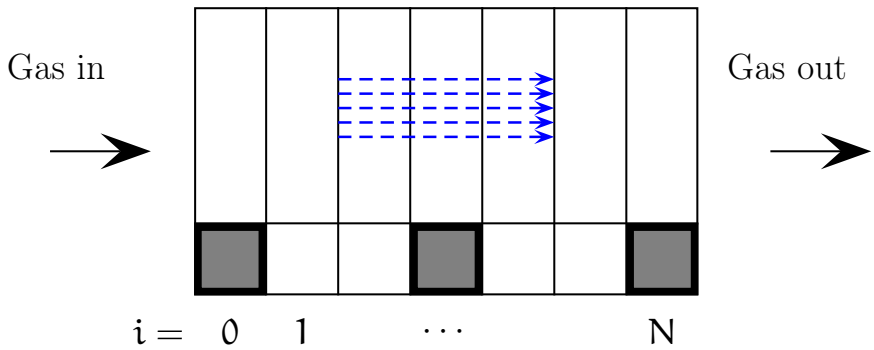

where we model advection using an upwinding finite difference approximation. In the solid segments, temperatures $T_{0,s}(t), \ldots, T_{N,s}(t)$ governed by

$$\rho_s c_s \frac{dT_{i,s}}{dt} = \frac{h}{l_s}(T_{i,g} - T_{i,s}) + \frac{\sigma\epsilon}{l_s}\left[\theta(x_i)T_{fce}^4 - (T_{i,s})^4\right], \tag{12a}$$

if i has a rod, and

$$T_{i,s}(t) = T_{i,g}(t), \tag{12b}$$

otherwise. The view factor θ is evaluated at the location of the ith segment $x_i := i\Delta x/N$.

Incrementing time windows The system of ODEs (11)–(12) holds within a given time window $t \in [0, t_w]$ during which the locations of the rods remain fixed. When we move to a new time window, the initial gas temperature $T_{i,g}(0)$ is set as the final value $T_{i,g}(t_w)$ from the previous window, and the initial solid temperature $T_{i,s}(0)$ is set as the final value of $T_{i+1,s}(t_w)$ from the previous

window (where the change in index i corresponds to the movement of the rods), for $i = 0, \ldots, N-1$. The last initial value for the next time window is $T_{N,s}(0)$, which we take to be ambient temperature T_{amb}. In addition, we relabel the rod indices i used to determine the case in (12) based on the new positions of the rods (adding a new rod at $i = N$ if necessary).

Quasi-steady state and example In the first time window, we use arbitrary initial conditions $T_{i,g}(0) = T_{\text{fce}}$ and $T_{i,s}(0) = T_{\text{amb}}$ for all i. As such, we are not interested in its performance in the first windows, where we have rods start part-way through the vestibule. We instead run the model for several time windows until we reach a quasi-steady state.

The full behaviour of this model (over 60 time windows of length 30 seconds) is shown in Figure 9, where we plot the gas and rod temperatures for every fourth rod over time. We track the temperature of each rod, which is not the same as $T_{i,s}$, as the rod locations i change between windows. We only plot every fourth rod, thereby reducing temperature overlaps for clarity. Transient effects from these arbitrary initial conditions are apparent during the first 10 minutes. After this time solutions are close to a quasi-steady state, in which the rod temperatures increase gradually from atmospheric temperature until they reach the end of the vestibule. The quasi-steady nature is visible in the gas temperature, where we see periodic behaviour. This periodicity corresponds to when each segment i has a rod (and so the gas transfers heat to the rod) or is empty (so no heat transfer from the gas occurs). The most important outputs from the model are not this full time evolution. Since we are interested in the efficiency of the vestibule, the key quantities of interest are the temperatures at which the gas leaves the vestibule (into the atmosphere) and the rods enter the furnace. To see this behaviour, in Figure 10 we plot the temperature of the gas (max/min/average over the final five time windows) and rod temperature versus location in the vestibule.

Figure 9: Evolution of gas and rod temperatures over time for the finite-width rod discretised model. The furnace temperature is taken to be equal to $1000\,\mathrm{K}$. We only plot every fourth value of i for clarity, removing plot overlaps. The view factor $\theta(x)$ is such that the function $\theta(x)T_f^4 = 0.4\,e^{-5x}$.

(a) Gas temperature $T_{i,g}$

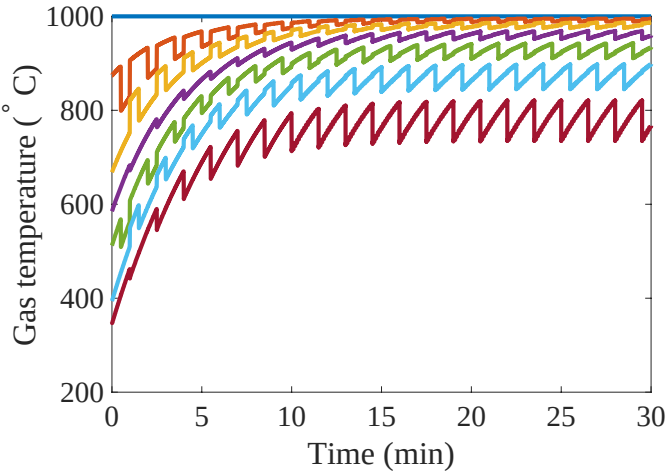

(b) Rod temperature $T_{i,s}$

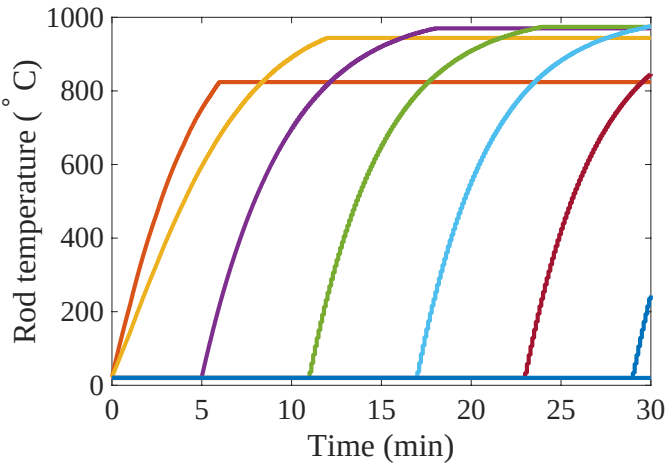

Figure 10: Gas and rod temperatures at each location in the vestibule for the finite-width rod discretised model. The left-hand end ($x = 0$) is the furnace and the right-hand end ($x = 0.5$) is the entrance to the vestibule.

(a) Gas temperature $T_{i,g}$

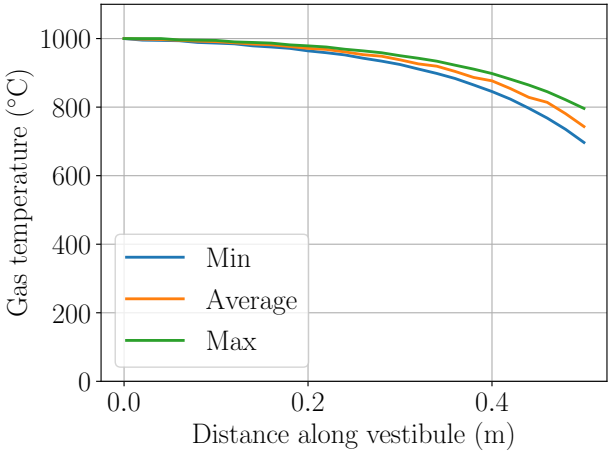

(b) Rod temperature $T_{i,s}$

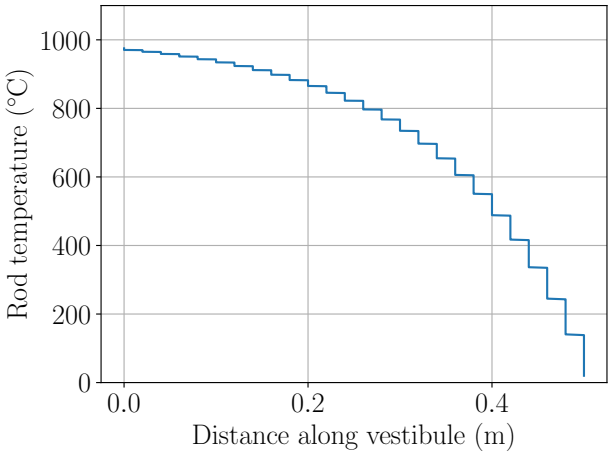

Numerical Results A nondimensional form of this model was solved numerically for a variety of rod and vestibule parameters, to examine the impact of vestibule design changes on heat efficiency of the furnace. Firstly, Figure 11 plots the exit gas temperature for 20 mm and 30 mm rod diameters (i.e. $l_s \in \{0.02, 0.03\}$) as a function of vestibule length, L. We see that longer vestibules tend to produce a lower gas exit temperature, and this relationship is clearer for larger rod diameters. Figure 12 examines this relationship more thoroughly. We see that longer vestibules are useful for lowering the exit gas temperature, and that this improvement is most apparent with larger rods, or when the rods are packed more tightly (e.g., every segment has a rod). This is intuitive, as it maximises the opportunity for heat exchange in the (limited) time it takes for the gas to advect to the exit of the vestibule. The incremental benefit of increasing the length of the vestibule is lower as the vestibule length increases. A vestibule length of 1–2 m appears to provide a suitable balance between efficiency and overall furnace length.

5 Heat transfer in the base

Previously, the models assumed some ideal conditions that may not be true in practice. Specifically, they assumed:

- heat transfer to the refractory base of the vestibule can be ignored;
- all gas entering the vestibule from the furnace is transported through the whole of the vestibule without any escape (leakage);
- gas enters the vestibule at the set temperature of the furnace (1050°C).

Instead, it may be that the following applies.

- There is non-trivial heat transfer between the gas in the vestibule and the refractory base material. This base provides the mechanism for stepping forward the bars into the furnace, and it is not monolithic. However, it is possible that heat can transfer to the base by

Figure 11: Gas exit temperature as a function of vestibule length for two rod sizes (lower indicates greater furnace/vestibule efficiency). Rods were positioned in every third segment.

(a) 20mm rod diameter

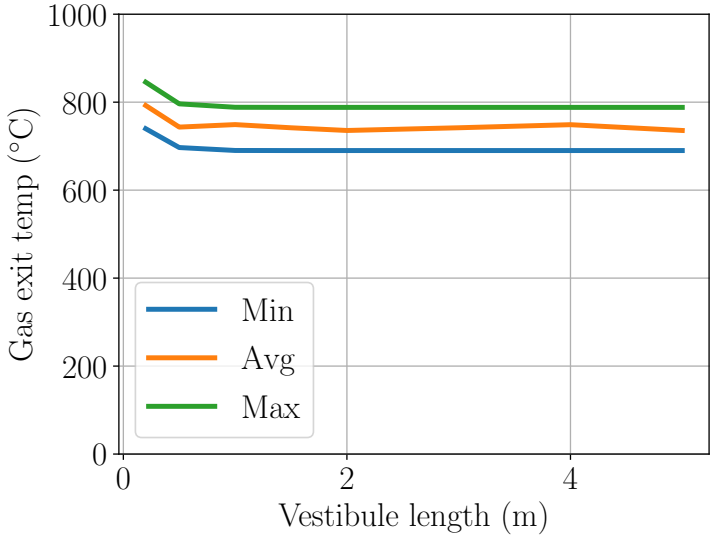

(b) 30mm rod diameter

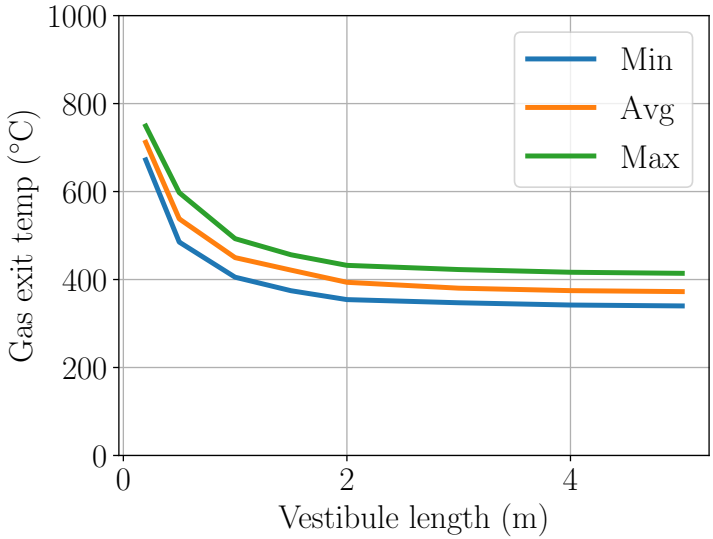

Figure 12: Gas exit temperature as a function of vestibule length in two studies: varying the rod diameter (left) and the frequency of rods (right) within segments (e.g., frequency 2 indicates every second segment i contains a rod). In the second study, the diameter of the rods were fixed at 20 mm.

(a) Varying rod diameter

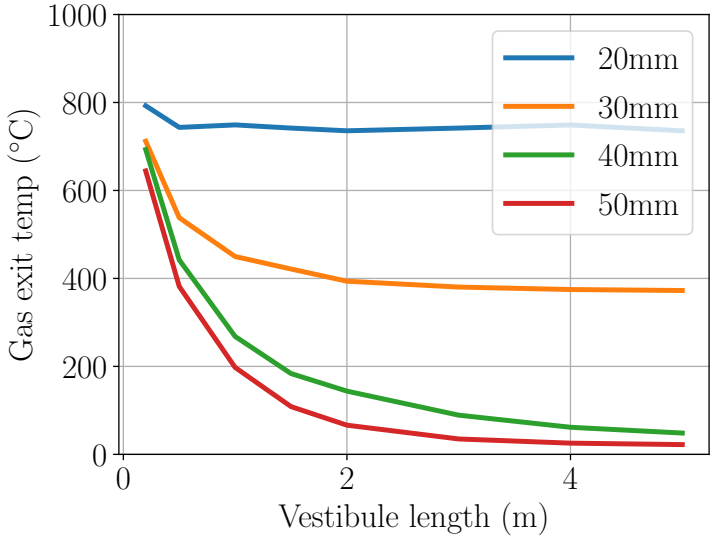

(b) Varying rod frequency

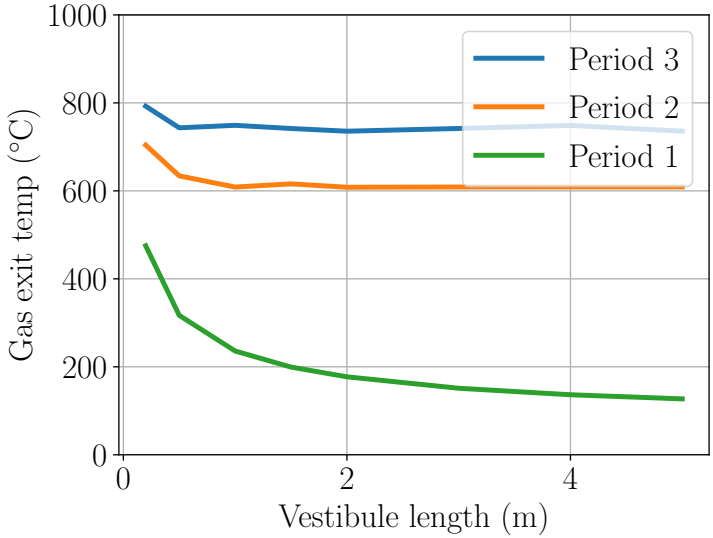

(a) convective heat transfer from the gas in the vestibule, via the spaces between bars,

(b) radiative heat transfer from the flame in the furnace, and

(c) conductive and radiative heat transfer from contact with the (presumably very hot) base of the furnace itself.

Moreover, the bars are in contact with the base material, so there is likely to be heat transfer between the base material and the rods.

- Because the vestibule base is not monolithic, there are likely to be gaps between its different components through which gas can escape. Also, there are definitely spaces at the (lateral) ends of the vestibule in the existing furnaces, which would also allow gas flowing through the vestibule to escape. These escape paths represent a loss of thermal mass, restricting the amount of heat that can be used to pre-heat the bars (and the base).

- There is some evidence, in the measured gas temperature data supplied by Lovells, that the temperature in the furnace, in the vicinity of the vestibule entrance, is less than the set temperature of the furnace. This may not be surprising, considering that the combustion source may not be uniform across the width of the furnace and that the vestibule is at the lower part of the furnace.

Finally, the previous models appear to require high heat transfer coefficients (≈ 100–$1000\,\mathrm{W\,m^{-2}\,K^{-1}}$) for heat transfer from gas to rods, while the expectation from Nusselt number correlations is that the heat transfer coefficient should be $\approx 1\,\mathrm{W\,m^{-2}\,K^{-1}}$. The aim of this work is to develop a model that incorporates heat transfer involving the base of the furnace/vestibule, gas loss (leakage) in the vestibule, gas temperature variation in the furnace and more realistic heat transfer coefficient (≈ 1–$10\,\mathrm{W\,m^{-2}\,K^{-1}}$) for heat transfer from the gas.

Figure 13: Schematic of the model geometry. The main difference from previous models is the inclusion of heat transfer in the base, extension of heat transfer into the furnace and gas leakage in the vestibule.

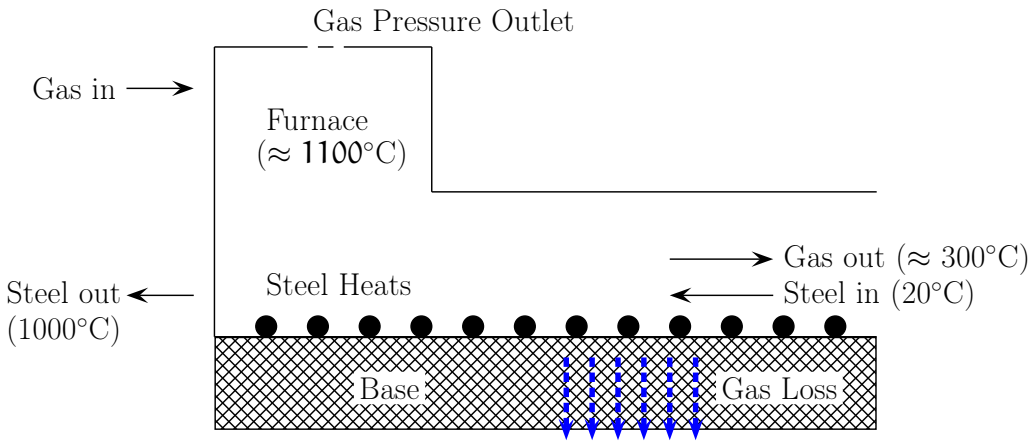

5.1 Model formulation

The model considers heat transfer from gas to bars, from gas to the base, radiation to bars and base, as well as heat transfer between base and bars. Also, the model extends into the furnace, assuming that the base is monolithic through both the vestibule and the furnace. Heat transfer is assumed to be by conduction in the base. Overall, the geometry of this model now resembles that in Figure 13.

The subsequent model has the following components. For the gas, conservation of mass (continuity) equation, including a gas loss term proportional to the mass flux of gas, gives

$$\frac{\partial\left(\rho_g u\right)}{\partial x} = -\frac{q_{loss}}{\ell_g}\rho_g u\,.$$

This equation is time independent, based on an assumption that the transit time for gas in the vestibule is a few seconds, compared to the transit time for a bar (minutes) and the heat conduction time in the base (hours). Heat conservation in the gas is

$$\rho_g c_g \left(\frac{\partial T_g}{\partial t} + u \frac{\partial T_g}{\partial x} \right) = \frac{h}{\ell_g} \left[\alpha \pi I(x)(T_s^k - T_g) + (1 - I(x))(T_b(x, 0) - T_g) \right] ,$$

where $I(x)$ is an indicator function, having the value 1 if there is a bar at location x, and value 0 otherwise, thus including heat transfer both to the bars and the base of the vestibule. The steel rods are assumed to be circular cylinders, with fraction α of their surface area in contact with the flowing gas, which is the reason for the $\alpha\pi$ coefficient in the above equation. In the results shown here $\alpha = 0.75$. For a particular bar in the vestibule/furnace with centre located at horizontal position x, denoted by index k, conservation of heat gives

$$\rho_s c_s \frac{dT_{s,k}}{dt} = \frac{4}{\pi \ell_s^2} \int_{x-\ell_s/2}^{x+\ell_s/2} \pi \left\{ \alpha \left[h(T_g - T_{s,k}) + \theta(x) \epsilon \sigma (T_{fce}^4 - T_{s,k}^4) \right] \right.$$
$$\left. + (1 - \alpha) h_b (T_b(x, 0) - T_{s,k}) \right\} dx \ .$$

The right-hand side is an integral because, in this model, the variation in gas flow and temperature, as well as the variation in the temperature of the base, is resolved at a scale finer than the size of the rods. The top two terms on the right-hand side represent convective heat transfer from the gas and radiative heat transfer from the furnace interior, while the bottom term represents heat transfer between the top surface of the base and the bottom part of the rod. This latter effect is likely to be a combination of conductive and radiative heat transfer, so a high heat transfer coefficient is used, $h_b = 1000\,\mathrm{W\,m^{-2}\,K^{-1}}$. The convective heat transfer coefficient h is assumed to take the form $h = h_0(u/u_0)^{1/2}$, in the vestibule, where u_0 is the gas speed entering the vestibule (taken to be $x = 1$), a form that comes from the Nusselt number correlation. The gas speed will vary because

(a) the gas cools down through the vestibule, increasing its density, and

(b) gas leakage.

In the following examples, $u_0 = 1\,\mathrm{m\,s^{-1}}$ and $h_0 = 10\,\mathrm{W\,m^{-2}\,K^{-1}}$. In the furnace itself we assume that there will be very vigorous gas activity, which is modelled by setting $h = 100\,\mathrm{W\,m^{-2}\,K^{-1}}$ therein. The view factor is taken to be 1 in the furnace, and to follow the form $\theta(x) = 1 - \left(\frac{2}{\pi}\tan^{-1} x\right)^{1/2}$ in the vestibule. In the case that any part of the vestibule is beyond a radiation shield, we assume that $\theta(x) = 0$, that is, the radiation shield is 100% effective. The form of the view factor is a simple heuristic and not necessarily accurate.

Heat transfer in the base is assumed to be by conduction, in two dimensions, thus the model equation for the base is

$$\rho_b c_b \frac{\partial T_b}{\partial t} = k_b \left(\frac{\partial^2 T_b}{\partial x^2} + \frac{\partial^2 T_b}{\partial z^2} \right),$$

with the boundary condition on the top surface being

$$-k_b \frac{\partial T_b}{\partial z}\bigg|_{z=0} = [1 - I(x)]h[T_g - T_b(x,0)] + I(x)(1-\alpha)h_b[T_{s,k} - T_b(x,0)].$$

Boundary conditions at the bottom and right-hand end of the base are assumed to be convective heat transfer to ambient temperature (taken to be 35 °C) and a no flux heat transfer condition at the left hand end (to represent the possibility that either the furnace extends further than the model or there is an insulated surface at the left-hand end). Initial conditions are that the base is at uniform temperature, being the ambient temperature, and that no bars exist inside the furnace or vestibule. The thermal properties of the refractory material comprising the base are taken to be $\rho_b = 2500\,\mathrm{kg\,m^{-3}}$, $c_b = 1000\,\mathrm{J\,kg^{-1}\,K^{-1}}$ and $k_b = 1\,\mathrm{W\,m^{-1}\,K^{-1}}$. The surface is taken to have emissivity $\epsilon = 0.1$.

5.2 Numerical solution

The heat equation in the base is discretised using a finite volume approach, with volume elements being square, of size $\Delta x \times \Delta x$. The gas equation is

discretised to correspond to the centre of the volume elements in the x-direction and backward first order differencing is used for the spatial derivatives. The time stepping is backward Euler, with time step Δt. Once the bars are introduced to the vestibule, they remain at one position for M time steps, where $M = \Delta x/(v_s\,\Delta t)$, and v_s is the average speed of the bars through the vestibule. After M time steps, the bars, and the corresponding indicator function, are moved one space to the left. This continues until bars exit the left end of the furnace.

In the results shown here, $\Delta x = 5\,\mathrm{mm}$, $\Delta t = 0.002\,\mathrm{s}$ and $v \approx 13.3\,\mathrm{cm\,min^{-1}}$ (which equates to moving 2 m in 15 s). The small time steps are required for stability of the explicit numerical scheme. For 25 mm diameter bars, each bar covers five spatial steps.

5.3 Results

Some sample results are shown here for the case of 25 mm rods, each having 50 mm spacing between them. Initially, the empty furnace and vestibule base is assumed to be at ambient temperature, then the base and vestibule are heated by radiation from the flame in the furnace at 1050 °C and convection heat transfer. Within the furnace, the gas temperature is assumed to vary as a quadratic, set to be 1050 °C at $x = 0$ and varying to closely fit two measured temperature values, as shown in Figure 14. The furnace gas temperatures are held at these values for the duration of each simulation. The temperature variation in the gas and base evolve according to the numerical scheme described above. After the initial two hour pre-heating, bars are introduced from the left end and their temperature is calculated as they move towards and into the furnace. Figure 14 shows a sample output from the model for a 50 cm length vestibule. In these simulations the dimensionless $q_{\mathrm{loss}} = 20$.

The results show that the gas temperature drops rapidly from about 150 mm into the vestibule. According to the model, the main reason for the rapid drop in gas temperature is the gas leakage. As a result, there is very little gas

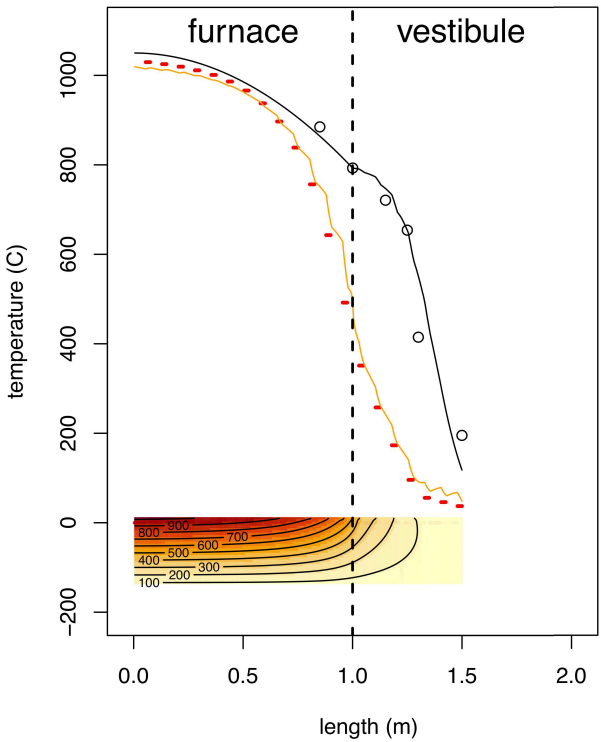

Figure 14: Model solution for a 50 cm long vestibule, with $q_{loss} = 20$, after six hours of simulation, including comparison with measured gas temperature data (black circles). The black line represents gas temperature, the orange line represents temperature of the top surface of the base and the red dots indicate rod temperatures. The temperature profile in the base is superimposed on the graph. The aspect ratio of the base has been altered to expand the vertical extent, in order to more clearly show the temperature variation.

exiting the vestibule. It is clear that there is reasonable agreement between the measured and calculated gas temperatures. For the rods, the temperature increases slowly initially, due to heat transfer from the gas and the base of the vestibule. Once the rods pass the radiation shield, there is a rapid increase in their temperature, closely matched by the surface temperature of the base. Eventually the rods reach just over 430 °C as they enter the furnace proper, where they more rapidly heat towards the target temperature. The effect of heating of the base, both within the furnace and along the length of the vestibule, is clear from Figure 14. Also, the effect of heat loss from the bottom and end of the base is evident. In this example, after six hours of operation, the maximum temperature in the base of the vestibule is around 500 °C, just

near the entrance to the furnace. It is evident that, overall, there is not much difference in temperature between the temperature of the rods and the top surface of the base, due to the high heat transfer between the two. Accordingly, about 55% of heat transferred from the gas by convection goes to the rods, with the remainder going to the base, indicating that heat transfer to the base is important in the overall heat transfer effects in the vestibule.

It is instructive to consider the same situation, but with no gas leakage, that is, $q_{loss} = 0$. The result of such a simulation is shown in Figure 15. The main difference in this result is that the gas temperature only drops to 715 °C by the end of the vestibule. Were gas to be exiting the vestibule at such a temperature, with a speed near $1\,\mathrm{m\,s^{-1}}$, it might be expected to be a hazardous situation. Due to the higher gas temperature and speed, there is more convective heat transfer to the rods, but the temperature of rods entering the furnace is only higher by about 55 °C, indicating that radiative effects appear to dominate.

Figures 16 to 19 show simulation results for four different vestibule lengths, ranging from the current length of 50 cm, up to 200 cm. In each case, $q_{loss} = 20$. It is clear from the longer lengths that gas leakage means that there is virtually no gas speed for lengths greater than about 50 cm, which means that there is effectively no heat transfer to the rods and base, because of the form of the heat transfer coefficient used in the model. In any case, this means that the extra vestibule length is not useful in capturing heat from the gas, because most of the gas has already leaked. Nevertheless, there is value in extending the vestibule length because more heat transfers through the base from the furnace, thus heating it up further and then transferring some of that heat to the rods. There is also more length available for radiative heat transfer to the rods and base from the flame in the furnace. In these simulations, a radiation shield is located 200 mm inwards from the outlet of the vestibule. It seems sensible to use as much of the vestibule length as possible to capture excess radiative heat, which can be transferred to the rods.

Figure 20 shows the calculated time variation of rod temperatures at the

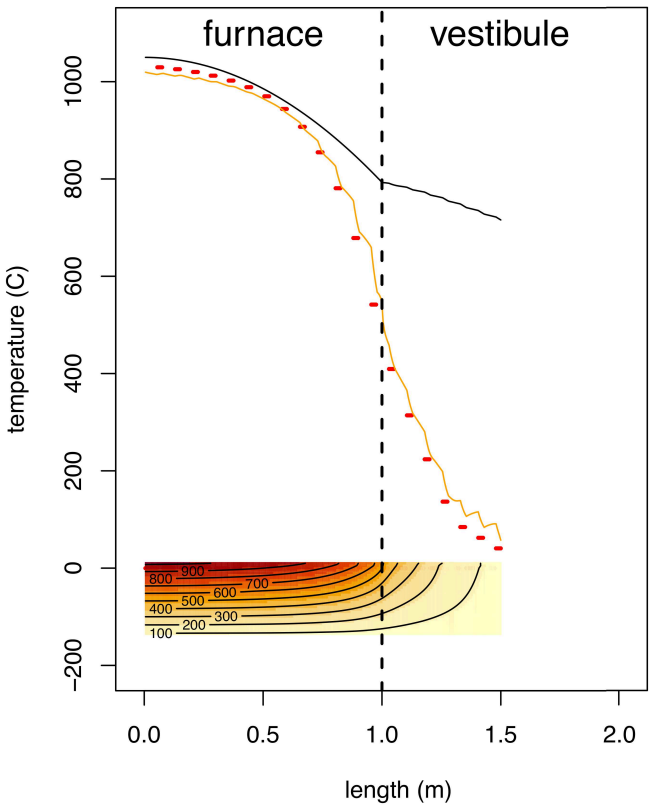

Figure 15: Model solution for a 50 cm long vestibule, with $q_{loss} = 0$, after six hours of simulation. The black line represents gas temperature, the orange line represents temperature of the top surface of the base and the red dots indicate rod temperatures. The temperature profile in the base is superimposed on the graph. The aspect ratio of the base has been altered to expand the vertical extent, in order to more clearly show the temperature variation.

point of entering the furnace. This value is a measure of the heat content that has been transferred to the rods during their transit through the vestibule. It shows a large increase in rod entry temperature by increasing the vestibule length to 100 cm, but smaller increases beyond that. The apparent sharp jump, especially for the 50 cm vestibule length, is continuous and smooth if viewed at a smaller scale near the time that rods begin to enter.

Figure 16: Model solution for vestibule length 50 cm. The black line represents gas temperature, the orange line represents temperature of the top surface of the base and the red dots indicate rod temperatures. The temperature profile in the base is superimposed on the graph. The aspect ratio of the base has been altered to expand the vertical extent, in order to more clearly show the temperature variation.

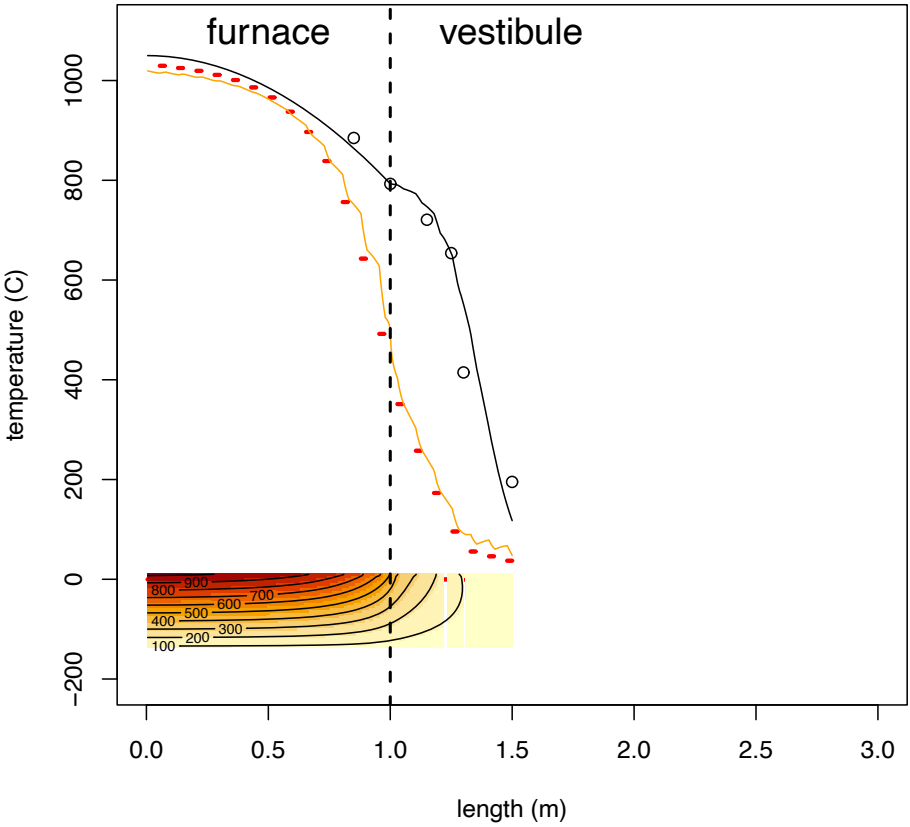

Figure 17: Model solution for vestibule length 100 cm. The black line represents gas temperature, the orange line represents temperature of the top surface of the base and the red dots indicate rod temperatures. The temperature profile in the base is superimposed on the graph. The aspect ratio of the base has been altered to expand the vertical extent, in order to more clearly show the temperature variation.

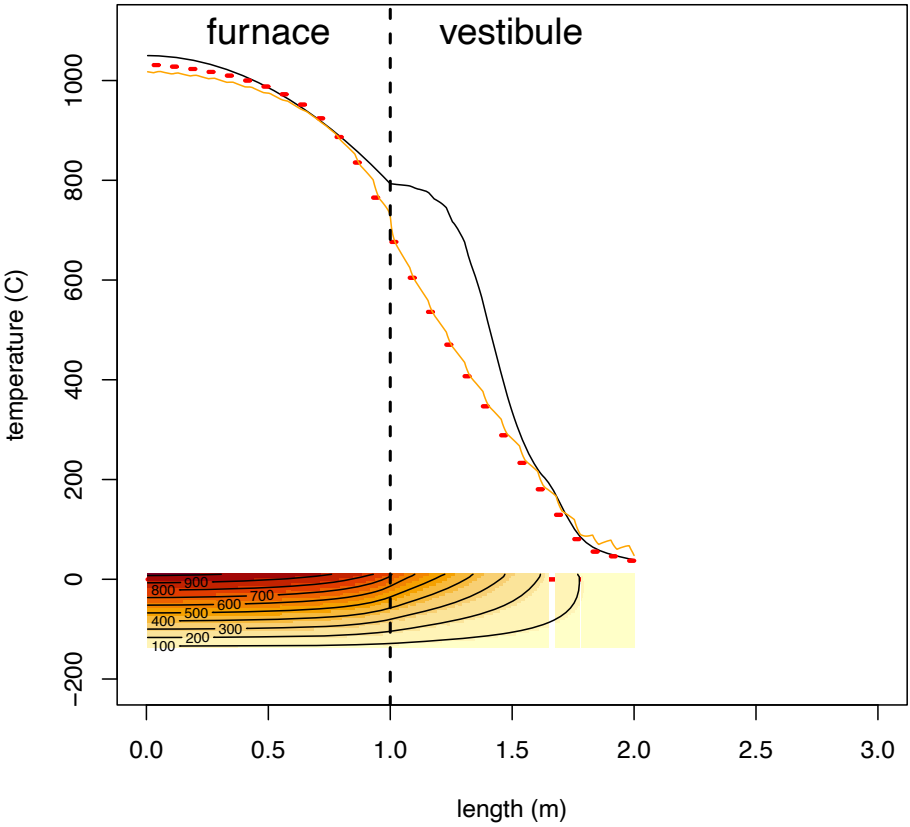

Figure 18: Model solution for vestibule length 150 cm. The black line represents gas temperature, the orange line represents temperature of the top surface of the base and the red dots indicate rod temperatures. The temperature profile in the base is superimposed on the graph. The aspect ratio of the base has been altered to expand the vertical extent, in order to more clearly show the temperature variation.

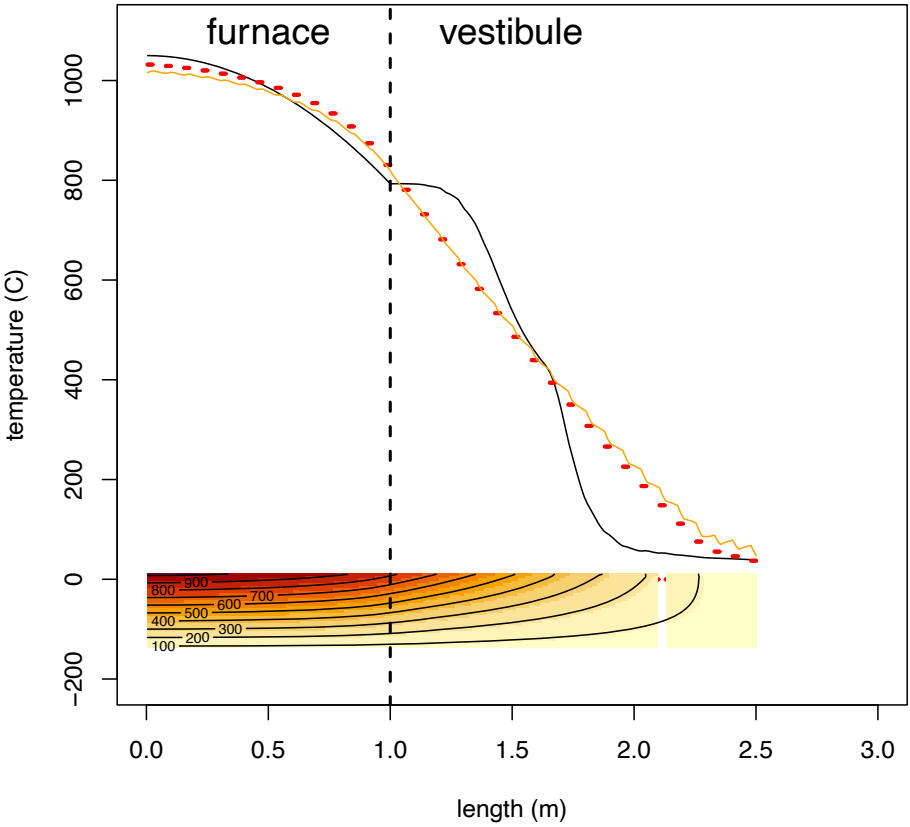

Figure 19: Model solution for vestibule length 200 cm. The black line represents gas temperature, the orange line represents temperature of the top surface of the base and the red dots indicate rod temperatures. The temperature profile in the base is superimposed on the graph. The aspect ratio of the base has been altered to expand the vertical extent, in order to more clearly show the temperature variation.

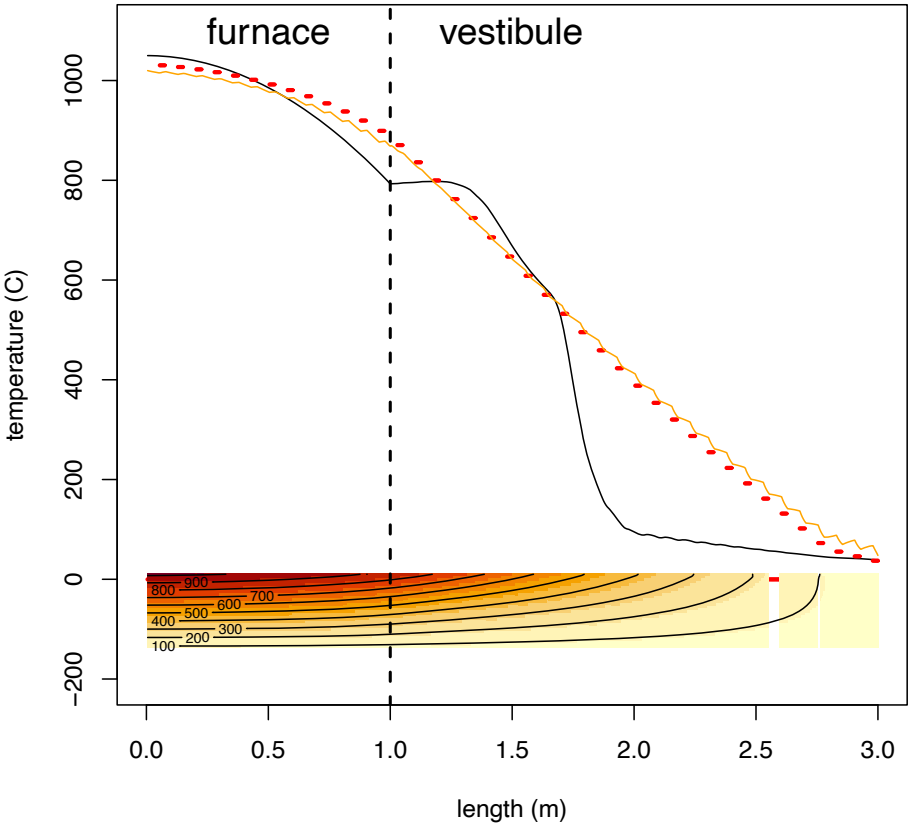

Figure 20: Time variation of the temperature at which rods enter the furnace, for different vestibule lengths (given in the legend). No rods enter the vestibule during the first two hours, which is meant to represent the heating up period in the morning. The rapid rises are not jumps, as temperatures are all continuous and single-valued in time.

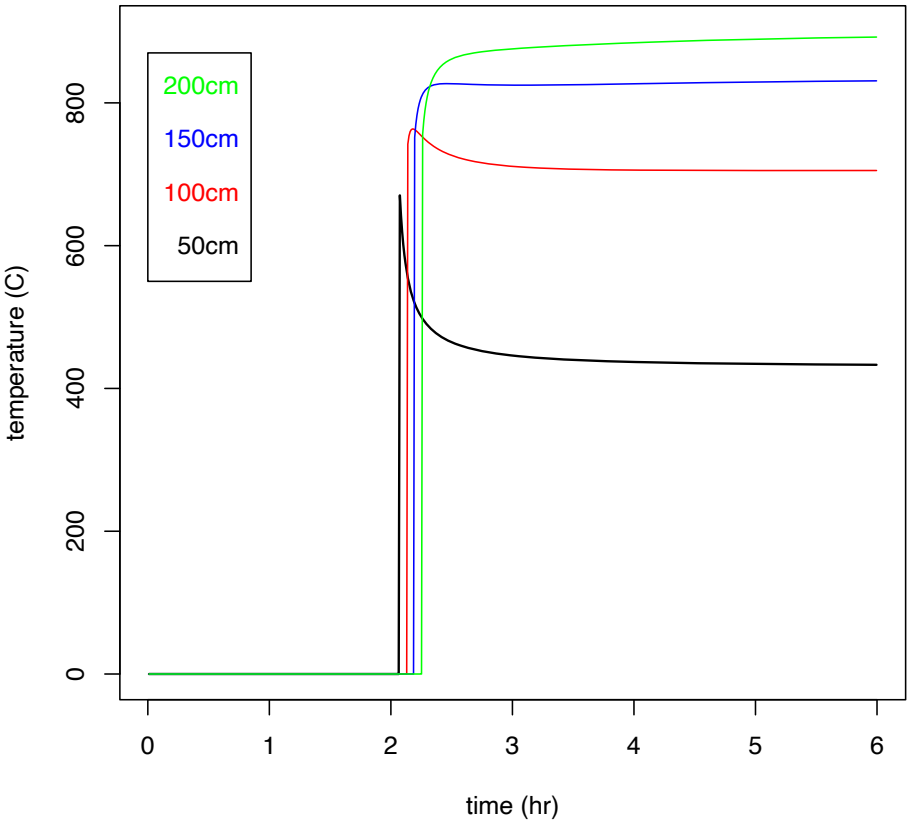

5.4 Conclusions

The key outcome from this particular modelling approach is that it is worth extending the vestibule from 50 cm to 100 cm, at least. There appear to be diminishing returns from further extensions to vestibule length. The key difference of this work to previous models is that the extension of the vestibule is justified by allowing more distance for rods to be heated by radiation from the furnace, combined with conduction/radiation from the vestibule base. This is in contrast to previous approaches, which were focused on heat recovery from the gas travelling through the vestibule. The results presented here show that it is unlikely that this latter effect can contribute significantly to pre-heating the rods because either

(a) gas leakage means that much of the sensible heat in the gas is lost, or

(b) the transit time of gas, combined with the low heat transfer coefficient means that little heat can be extracted, if there is no gas leakage.

There are several reasons why this model may not be accurate:

- the various parameters (material properties, heat transfer coefficients, etc) used in the model are only rough estimates, and may not be correct;
- there may not be good connection between the base of the vestibule and that of the furnace, which may affect the heat transfer between them;
- the model for gas leakage is very approximate;
- the view factor function used may be a poor approximation to reality.

If desired, then each of these factors could be examined more carefully, in order to improve the model. Moreover, by extending the model to include heating in the furnace, it may be a useful tool for some simulation experiments during the design process for new furnaces.

Figure 21: Some of our group visited the Lovells factory. A heated rod is being twisted into a coil at bottom left, and bottom right is a view inside the furnace with several heated rods visible.

6 Conclusions

Several models of heat transport in the vestibule of a furnace that heats steel rods to a malleable temperature, ranging from simple to more realistic, have been proposed and solved. The purpose of the modelling was to guide decisions about future design of the vestibule, especially its length, in order to reduce energy usage by preheating rods as they enter the furnace. The mechanisms of radiative and convective heat transfer were allowed for, and the discrete nature of the rods and the way they are advanced through the vestibule was allowed for in the most advanced of the models.

The present length of a vestibule is of the order of half a metre. Model results indicate that for rods with thicknesses less than 25 mm there is little improvement in heating economy to be gained by increasing vestibule length. For thicker rods, increasing this length to one or two metres provides significant extra preheating of rods by the hot gases that exit through the vestibule, and by the radiation that escapes to the vestibule.

Acknowledgements A large and lively group of mathematicians worked on this challenge during the Study Group week, many of whom are listed as authors, but also including Joshua Connor, Pierluigi Cesana, and Raju Chowdhury, to whom we are grateful for their contributions.

We are especially grateful to Simon Crane from Lovells Coils for bringing this challenge and his energy and experience to the Study Group, and to the Applied Mathematics group at the School of Mathematical and Physical Sciences, University of Newcastle, for providing the resources and such a friendly environment to host this Mathematics in Industry Study Group.

References

Bird, R. Byron, Warren E. Stewart, and Edwin N. Lightfoot (2002). *Transport Phenomena*. Second Edition. John Wiley & Sons (cit. on p. M126).

Gupta, G.P. and S.C. Saxena (1970). "Thermal conductivity of carbon dioxide in the temperature range 100 deg C to 1075 deg C". In: *Molecular Physics* 19.6, pp. 871–880. DOI: 10.1080/00268977000101881 (cit. on pp. M122, M123).

Sweatman, W.L., S.I. Barry, and M. McGuinness (2012). "Heat Transfer During Annealing of Steel Coils". In: *Progress in Industrial Mathematics at ECMI 2010. Mathematics in Industry*. Ed. by M. Günther et al. Vol. 17. Berlin, Heidelberg: Springer. DOI: 10.1007/978-3-642-25100-9_35 (cit. on p. M123).

Author addresses

(a) **M. J. McGuinness**, School of Mathematics and Statistics, Victoria University of Wellington, PO Box 600, Wellington, 6140 New Zealand
mailto:mark.mcguinness@vuw.ac.nz
orcid:0000-0003-1860-6177

(b) **B. J. Cox**, School of Mathematical Sciences, University of Adelaide, South Australia 5005, Australia.
mailto:barry.cox@adelaide.edu.au
orcid:0000-0002-0662-7037

(c) **B. Kalyanaraman**, School of Mathematical and Physical Sciences, University of Newcastle, Callaghan, NSW 2308, Australia
mailto:balaje.kalyanaraman@newcastle.edu.au

(d) **K. B. Kiradjiev**, Mathematical Institute, University of Oxford, United Kingdom.
mailto:kiradjievk@gmail.com
orcid:0000-0002-4716-0330

(e) **R. Gonzalez-Farina**, School of Mathematics, Cardiff University, Cardiff, CF24 4AG United Kingdom
mailto:gonzalezfarinar@cardiff.ac.uk
orcid:0000-0001-6116-0807

(f) **C. Z. W. Hassell Sweatman**, School of Engineering, Computer and

Mathematical Sciences, Auckland University of Technology, Auckland 1010, New Zealand.
mailto:catherine.sweatman@aut.ac.nz
orcid:0000-0002-1616-8209

(g) **Lindon Roberts**, Mathematical Sciences Institute, Australian National University, Canberra, ACT 2601, Australia.
mailto:lindon.roberts@anu.edu.au
orcid:0000-0001-6438-9703

(h) **D. I. Pontin**, School of Mathematical and Physics Sciences, University of Newcastle, Callaghan, NSW 2308, Australia.
mailto:david.pontin@newcastle.edu.au
orcid:0000-0002-1089-9270

(i) **Edward J. Bissaker**, School of Mathematical and Physcial Sciences, The University of Newcastle, New South Wales 2308, Australia.
mailto:edward.bissaker@uon.edu.au
orcid:0000-0002-1608-286X

(j) **S. K. Irvine**, School of Fundamental Sciences, Massey University, New Zealand
mailto:samuelkyleirvine@gmail.com

(k) **D. R. Jenkins**, School of Engineering, The University of Newcastle, NSW, Australia.
mailto:David.Jenkins@newcastle.edu.au
orcid:0000-0001-9660-0585

(l) **I. J. Taggart**, School of Engineering, The University of Newcastle, NSW, Australia.
mailto:Ian.Taggart@newcastle.edu.au
orcid:0000-0003-1587-5427